Stem Cell Reports
Article

ISSCR

OPEN ACCESS

Establishment of a Human Blood-Brain Barrier Co-culture Model Mimicking the Neurovascular Unit Using Induced Pluri- and Multipotent Stem Cells

Antje Appelt-Menzel,[1,2] Alevtina Cubukova,[2] Katharina Günther,[3] Frank Edenhofer,[3,4] Jörg Piontek,[5] Gerd Krause,[6] Tanja Stüber,[7] Heike Walles,[1,2] Winfried Neuhaus,[8,9] and Marco Metzger[1,2,9,*]

[1]University Hospital Würzburg, Chair Tissue Engineering and Regenerative Medicine, 97070 Würzburg, Germany
[2]Translational Center Würzburg "Regenerative Therapies for Oncology and Musculoskeletal Diseases", Branch of Fraunhofer Institute for Interfacial Engineering and Biotechnology IGB, 97070 Würzburg, Germany
[3]Julius-Maximilians-University Würzburg, Institute of Anatomy and Cell Biology, Stem Cell and Regenerative Medicine Group, 97070 Würzburg, Germany
[4]Leopold-Franzens-University Innsbruck, Institute of Molecular Biology & CMBI, Department Genomics, Stem Cell Biology & Regenerative Medicine, 6020 Innsbruck, Austria
[5]Charité Universitätsmedizin Berlin, Clinical Physiology & Nutritional Medicine, Department of Gastroenterology, Rheumatology & Infectious Diseases, 12203 Berlin, Germany
[6]Leibniz Institut für Molekulare Pharmakologie, 13125 Berlin, Germany
[7]University Hospital Würzburg, Women's Hospital and Polyclinic, 97080 Würzburg, Germany
[8]AIT Austrian Institute of Technology GmbH, Competence Center Health and Bioresources, Competence Unit Molecular Diagnostics, 1190 Vienna, Austria
[9]Co-senior author
*Correspondence: marco.metzger@igb.fraunhofer.de
http://dx.doi.org/10.1016/j.stemcr.2017.02.021

SUMMARY

In vitro models of the human blood-brain barrier (BBB) are highly desirable for drug development. This study aims to analyze a set of ten different BBB culture models based on primary cells, human induced pluripotent stem cells (hiPSCs), and multipotent fetal neural stem cells (fNSCs). We systematically investigated the impact of astrocytes, pericytes, and NSCs on hiPSC-derived BBB endothelial cell function and gene expression. The quadruple culture models, based on these four cell types, achieved BBB characteristics including transendothelial electrical resistance (TEER) up to 2,500 Ω cm^2 and distinct upregulation of typical BBB genes. A complex in vivo-like tight junction (TJ) network was detected by freeze-fracture and transmission electron microscopy. Treatment with claudin-specific TJ modulators caused TEER decrease, confirming the relevant role of claudin subtypes for paracellular tightness. Drug permeability tests with reference substances were performed and confirmed the suitability of the models for drug transport studies.

INTRODUCTION

The blood-brain barrier (BBB) is the most important biological barrier between the blood circulation and the central nervous system (CNS), consisting of specialized blood endothelial cells (ECs) that line the cerebral capillaries and are connected by very dense tight junctions (TJs). Anatomically, the BBB is part of the neurovascular unit, which maintains the physiological function of the brain capillary ECs and includes cellular components such as pericytes, astrocytes, neurons, and microglia (Hawkins and Davis, 2005). The main functions of the BBB are the maintenance of CNS homeostasis and the prevention of penetration of neurotoxic substances as well as pathogens, such as bacteria and viruses. Besides functioning as a physical barrier, the BBB plays a major role as a transport and metabolic barrier (Neuhaus and Noe, 2010).

Models of the BBB serve as very strong tools in drug development and are important to elucidate further physiological and pathophysiological molecular mechanisms. Besides in silico and in vivo models, a variety of cellular in vitro BBB models are available, such as transwell models, dynamic flow-based hollow-fiber models, or microfluidic devices (Avdeef et al., 2015). So far, primary porcine, bovine, and rodent ECs are characterized by the best functionality, tightest barrier integrity, and lowest permeability (Vastag and Keseru, 2009). Disadvantages associated with the use of primary cells are the time- and cost-intensive isolation processes, the variabilities between cells of different isolations, and the high consumption of animals for each new isolation. Access to human primary brain material is very limited and restricted to biopsy or autopsy material from patients with diseases such as epilepsy or brain tumors. The use of EC lines for BBB modeling helps to circumvent the disadvantages of primary cells. Immortalized cells of different species, such as murine EC lines (MBEC4, b.END3, b.END5, cEND, cerebEND) as well as cell lines from rat (RBE4), cow (t-BBEC-117), pig (PBMEC/C1-2), and human (hCMEC/D3, hBMEC, TY10, and BB19) exist (Eigenmann et al., 2013; Avdeef et al., 2015). These cell lines have the advantage of being usable over many passages with a higher reproducibility of the results compared with primary cells. Notably, almost all immortalized cell lines form barriers with a transendothelial electrical resistance (TEER) below 150 Ω cm^2 (Deli et al., 2005). For drug transport and barrier functionality studies, a minimal tightness of the BBB models with TEER values between 150 and 200 Ω cm^2 has been defined (Gaillard and de Boer, 2000). However, compared with physiological TEER values of more than 1,500 Ω cm^2, which have been measured in

capillaries of rat or frog brains (Crone and Olesen, 1982; Butt et al., 1990), the discrepancies with current in vitro models are significant. Another important aspect is the species differences that exist between humans and other mammalian subsets. In particular, the expression and functionality of important BBB transporters such as P-glycoprotein are described (Takeuchi et al., 2006; Warren et al., 2009).

Therefore, there is a significant need for adequate human BBB models for academic research and the pharmaceutical industry. Minimal requirements would be the reproducibility of results, characteristic permeability of reference components, expression of main BBB transporters, and physiological cell morphology (Cecchelli et al., 2007).

In recent promising studies, various stem cell types have been used as an alternative source for BBB remodeling. Stem cells are self-renewable, can be subsequently differentiated into mature somatic cell types, and serve as a virtually unlimited independent cell source. In particular, hematopoietic stem cells from human umbilical cord blood (Cecchelli et al., 2014), circulating endothelial progenitor cells mobilized from bone marrow (Boyer-Di Ponio et al., 2014), as well as human induced pluripotent stem cells (hiPSCs) (Lippmann et al., 2012) have been used for BBB modeling with promising in vivo-like characteristics, e.g. TEER values up to 5,000 Ω cm^2 (Lippmann et al., 2014). The addition of stimulating compounds such as retinoic acid (RA) during differentiation (Lippmann et al., 2014) and co-culturing with individual niche cell types, such as pericytes, astrocytes, and neural cells, have further improved BBB properties (Lippmann et al., 2013; Cecchelli et al., 2014).

The aim of this study was to systematically investigate the individual impact of the different cell types on hiPSC-derived BBB endothelial cell (hiPS-EC) function as well as gene expression and therefore establish the most predictive BBB model. Furthermore, we standardized the methods to differentiate the corresponding BBB cell types from hiPSCs as well as human multipotent stem cells. Thus, it will be technically feasible to generate large quantities of human cell types from a single cell source and, in combination with new detection methods, to develop standardized higher-throughput in vitro assays in drug discovery and toxicity testing.

RESULTS

Characterization of Multipotent and Pluripotent Stem Cells Used for BBB Modeling

hiPSCs as well as multipotent neural stem cell (NSCs) provide an effective cell source to generate functional brain cells and have the advantage of being independent of postnatal brain tissue biopsy samples. For our studies, we used the recently published hiPSC lines IMR90-4 and ARiPS (Kadari et al., 2014) to differentiate them into BBB ECs (Lippmann et al., 2012) and hiPS-NSCs. As a physiological control, NSCs were additionally isolated from fetal brain tissue (fNSCs). The growth characteristics of hiPSCs are similar to embryonic stem cells, forming compact colonies with defined borders, which typically appear in phase-contrast microscopy (Figure 1D). Colonies were characterized by immunofluorescence staining for pluripotency-associated markers, including OCT3/4 (Figure 1A), SOX2 (Figure 1B), and TRA1-81 (Figure 1C); flow cytometry analyses demonstrated at least 90% positive staining (data not shown). For differentiation of hiPSCs into NSCs, a recently published protocol was used employing neurogenic media in adherent culture (Yan et al., 2013) with slight modifications described by Günther et al. (2016). Morphology of hiPS-NSCs (Figure 1H) appeared as typical rosette-like structures, whereas fNSCs (Figure 1L) were more heterogeneous, some of them with elongated processes. After culturing both NSC types in NSC medium containing basic fibroblast growth factor (bFGF) and epidermal growth factor (EGF), NSCs could be further expanded in vitro. NSC identity was confirmed by staining for early NSC markers such as SOX1 (Figures 1E and 1I), SOX2 (Figures 1F and 1J), and NESTIN (Figures 1G and 1K). In contrast, the expression of pluripotency and astroglial markers could not be detected (data not shown).

Characterization of Differentiated BBB Cell Types

For differentiation of hiPSCs and NSCs to BBB ECs and astrocytes, the in vivo neurodevelopmental process has to be mimicked in vitro. For BBB capillary ECs, a co-differentiation of neural and ECs was initiated by treatment with a so-called unconditioned medium (Lippmann et al., 2014). The purification of hiPS-ECs was performed using an EC medium with RA and sub-cultivation on a collagen IV-/fibronectin-coated matrix. After differentiation for 10 days, hiPS-ECs showed a typical elongated spindle-shaped morphology, and the cell size was increased compared with the original hiPSCs (Figure 2A). The hiPS-ECs were characterized by immunofluorescence staining for the typical EC marker von Willebrand factor (vWF, Figure 2B). The TJ-associated protein ZO1 as well as the BBB-relevant glucose transporter 1 (GLUT1) were homogeneously expressed at the cell-cell borders (Figures 2C and 2D). The expression of the adherence junction protein vascular endothelial cadherin (CDH5) was also detectable, the endothelial proteins angiopoietin receptor 2 (TIE2) and PECAM1 (CD31) appeared weaker and less distinct (Figures S1A–S1C). The functionality of the hiPS-ECs was tested by an uptake assay with fluorescein isothiocyanate (FITC)-labeled acetylated low-density lipoprotein. Substance was taken up by 92.4% of the BBB hiPS-ECs (Figure S1D), and

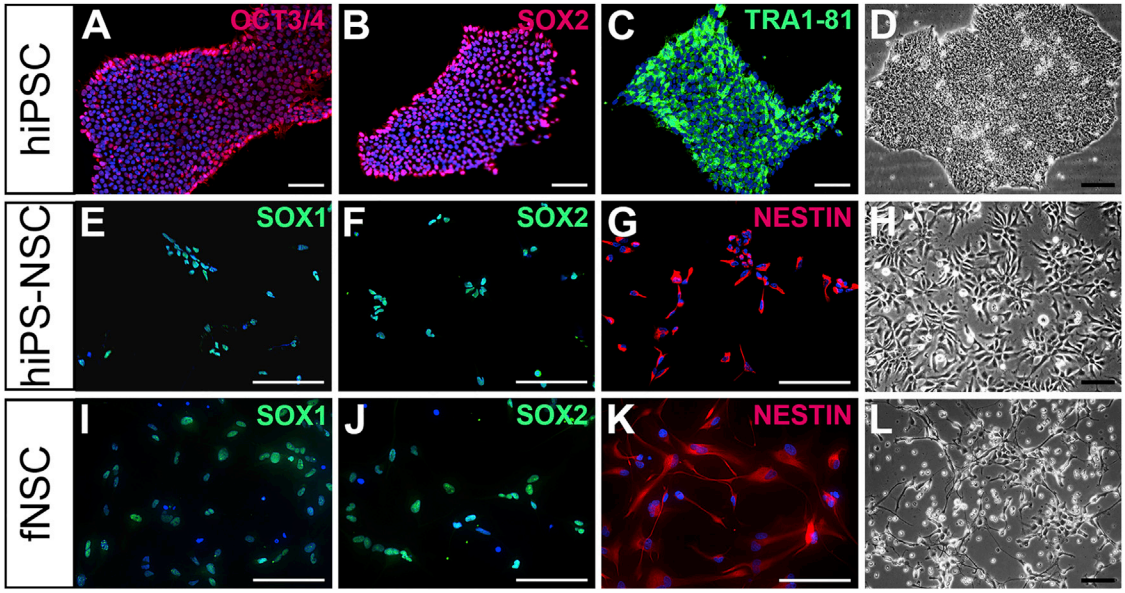

Figure 1. In Vitro Characterization of Pluripotent and Multipotent Stem Cells

(A–C, E–G, and I–K) Immunofluorescence staining of characteristic pluripotent stem cell (A–C) and NSC (E–G and I–K) markers. hiPSCs express OCT3/4 (A), SOX2 (B), and TRA1-81 (C), NSCs express SOX1 (E and I), SOX2 (F and J), and NESTIN (G and K). Cell nuclei were stained with DAPI in blue.

(D, H, and L) Phase-contrast image of hiPSCs (D), NSCs differentiated from hiPSCs (H; hiPS-NSC) and NSCs isolated from fetal brain tissue (L; fNSC).

Scale bars, 100 μm.

the fluorescence intensity was lower compared with the control cell line, human umbilical vein endothelial cells (Figures S1D–S1F).

Astrocytes differentiated from hiPSCs (hiPS-As, Figures 2E–2H) as well as human primary fetal brain astrocytes from the cerebral cortex (astrocytes, Figures 2I–2L) were characterized by immunofluorescence staining for intermediate filament protein glial fibrillary acidic protein (GFAP, Figures 2F and 2J) as well as for glial-specific calcium-binding protein B (S100β, Figures 2G and 2K). The differentiation efficiency of hiPSCs, analyzed by flow cytometry, was relatively high with 53.8% GFAP-positive astrocytes (H), although human primary fetal brain astrocytes were nearly 100% positive for GFAP (L).

As for astrocytes, human primary pericytes were heterogenic in their morphology and marker expression. Cells showed elongated fibroblast- or MSC-like morphology and were positively stained for alpha smooth muscle actin (αSMA, Figure 2N) and platelet-derived growth factor receptor-beta (PDGFRβ, Figure 2O). Flow cytometry demonstrated 85.2% PDGFRβ-positive cells (Figure 2P).

BBB Modeling and Tightness Characterization

To investigate the influence of different cell types on BBB hiPS-EC integrity, diverse sets of BBB co-cultures were established. As shown in Figure 3A, the differentiated hiPS-ECs were cultured on a collagen IV-/fibronectin-coated transwell membrane. The different types of co-culture cells were seeded in coated wells in the bottom compartment without direct contact with the hiPS-ECs. We studied the influence of primary fetal brain astrocytes, hiPS-As, primary fetal brain pericytes, and NSCs derived from hiPSCs (hiPS-NSCs) or isolated from fetal brain (fNSCs) on BBB hiPS-EC integrity. Moreover, we established several combinations of the above-mentioned cell types to study synergistic effects.

After 2 days of co-culture, the TEER was measured as the first important readout characterizing the paracellular tightness of hiPS-ECs. The cell density of co-culture cells was kept constant independent from the co-culture system. A significant increase in TEER compared with the hiPS-EC monocultures (TEER = 1,198 ± 265) could be obtained by triple culture of hiPS-ECs, hiPS-NSCs, and pericytes (1,723 ± 90 Ω cm^2) as well as by quadruple culture of hiPS-ECs, hiPS-NSCs, astrocytes, and pericytes (1,757 ± 320 Ω cm^2) (Figure 3B). Maximal absolute TEER values ranged between 2,000 Ω cm^2 (mono-culture) and 2,500 Ω cm^2 (triple and quadruple culture), approximately (Figure 3C).

In addition to TEER measurements, we analyzed BBB models according to a characteristic gene expression profile

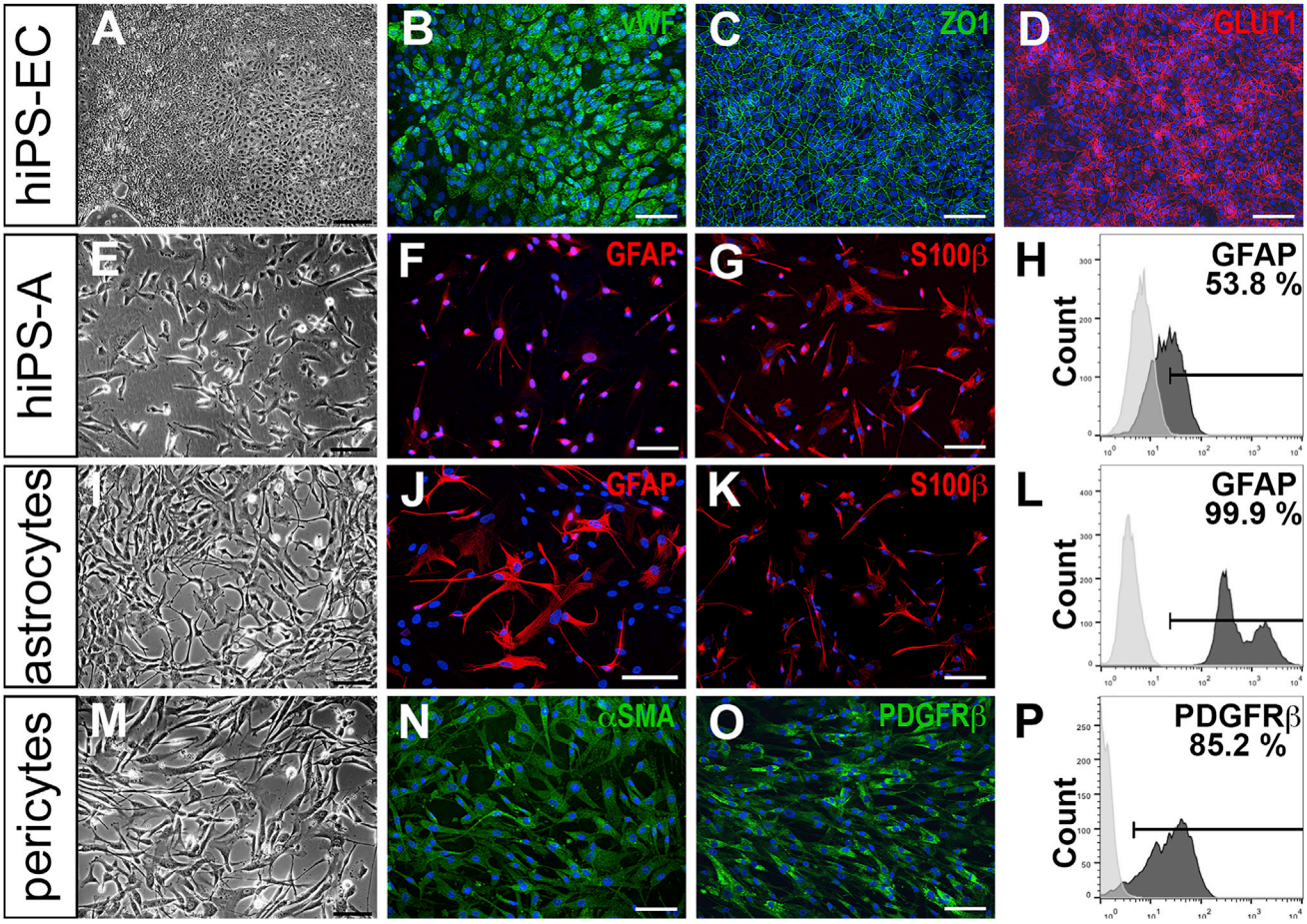

Figure 2. In Vitro Characterization of Differentiated BBB-Relevant Cell Types

(A, E, I, and M) Phase-contrast image of BBB ECs differentiated from hiPSCs: hiPS-ECs (A), astrocytes differentiated from hiPSCs (hiPS-As) (E), human primary brain astrocytes (I), and pericytes (M).

(B–D) Immunofluorescence staining of characteristic EC markers vWF (B), TJ-associated protein ZO1 (C), and glucose transporter GLUT1 (D). For further characterization, see also Figure S1.

(F–H, J–L, and N–P) The astrocytic proteins GFAP (F and J) and S100β (G and K) were expressed by hiPS-A as well as by human primary brain astrocytes. Human primary brain pericytes were characterized by staining for αSMA (N) and PDGFRβ (O). Cell nuclei were stained with DAPI in blue. Fluorescence-activated cell sorting analysis of astrocytic protein GFAP (H and L) and pericyte marker PDGFRβ (P) reveals quantification of 53.8% GFAP-positive hiPS-As (H), 99.9% GFAP-positive primary astrocytes (L), and 85.2% primary pericytes.

Scale bars, 100 μm.

via qRT-PCR. Genes included the efflux transporter *ABCB1*, the glutamate transporter *SLC1A1*, the glucose transporter *SLC2A1*, and TJ component *OCLN*. The hiPS-EC mono-culture (100%) was compared with the different co-culture settings (Figure 3D), and a 1.5-fold regulation in gene expression was set as an arbitrary biological threshold. In concordance with the TEER experiments, the most robust upregulation was observed for the quadruple culture, indicating effective modeling of the BBB phenotype. Under these conditions, the expression of *ABCB1* was on average upregulated by 1.5-fold, *SLC1A1* by 1.3-fold, *SLC2A1* by 1.7-fold, and *OCLN* by 1.6-fold compared with hiPS-ECs from mono-cultures, however statistical significance was reached only for *SLC2A1*. The triple culture of hiPS-ECs, hiPS-NSCs, and pericytes revealed only moderate upregulation of 1.3-fold for *ABCB1*, 1.5-fold for *SLC1A1*, 1.2-fold for *SLC2A1*, and 1.4-fold for *OCLN*. Other co-culture systems also yielded moderate upregulation in expression of these genes, however, with higher variances as in the quadruple culture. Noteworthy, no significant effects were observed on gene expression and TEER of hiPS-ECs using the control colon carcinoma cell line Caco-2 (data not shown).

As the quadruple culture showed the strongest enhancement of the phenotypical development of BBB properties,

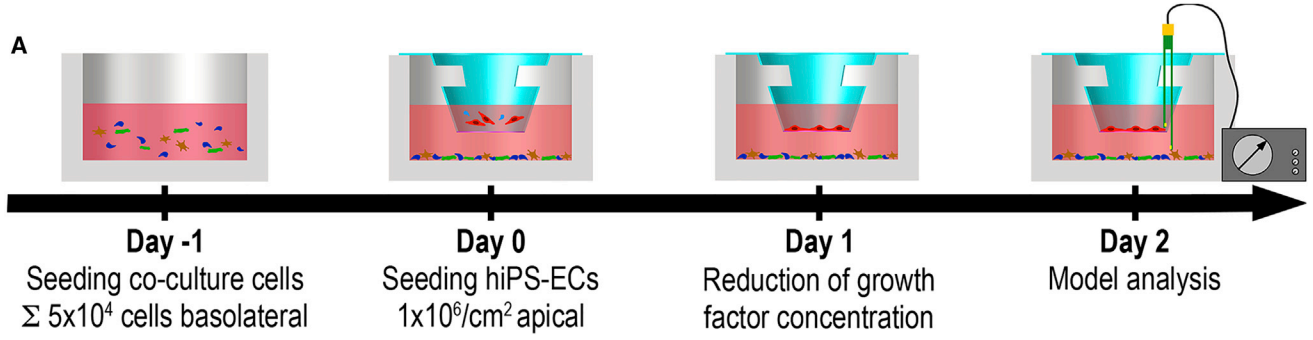

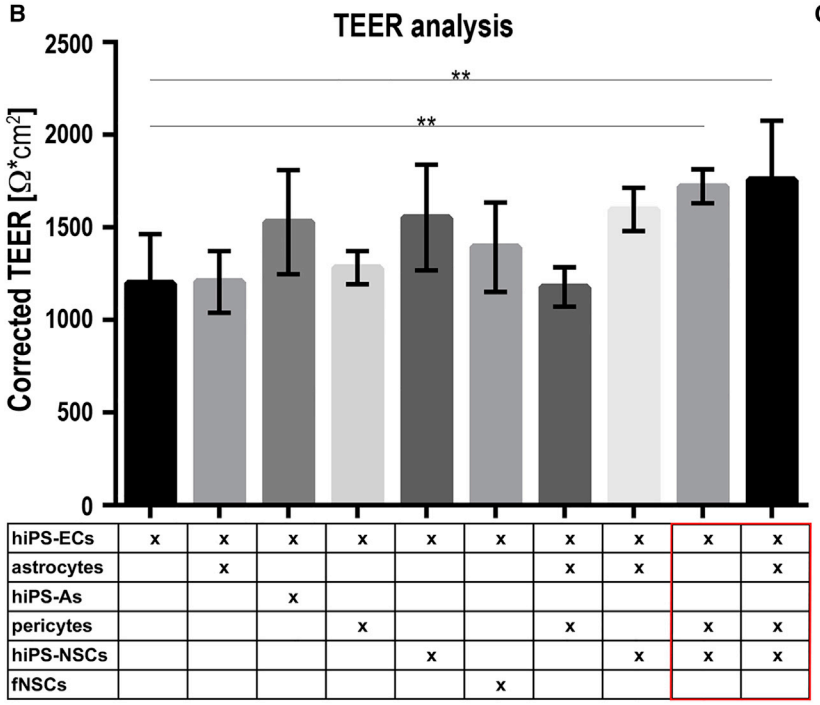

C

Culture system	TEER [Ω*cm²] Minimal values	Maximal values
Mono-culture		
hiPS-ECs	631	2073
Co-culture		
+ astrocytes	405	2024
+ hiPS-A	534	2485
+ pericytes	474	2107
+ hiPS-NSCs	432	2171
+ fNSCs	408	2482
Triple culture		
+ astrocytes + pericytes	391	2105
+ astrocytes + hiPS-NSCs	748	2293
+ pericytes + hiPS-NSCs	810	2556
Quadruple culture		
+ astrocytes + pericytes + hiPS-NSCs	433	2489

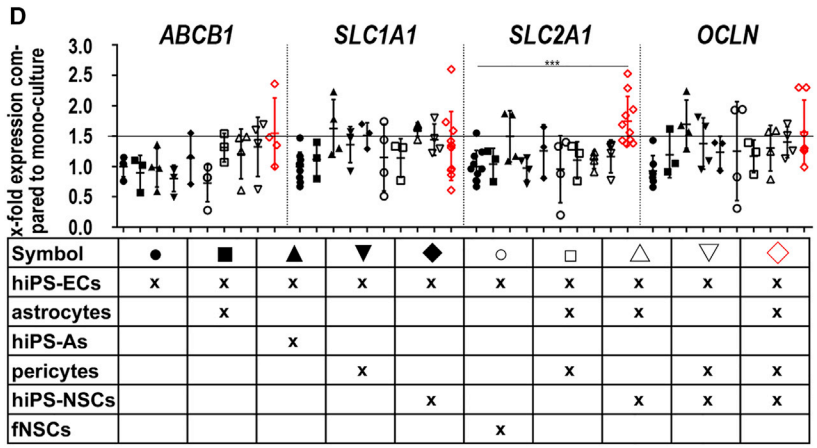

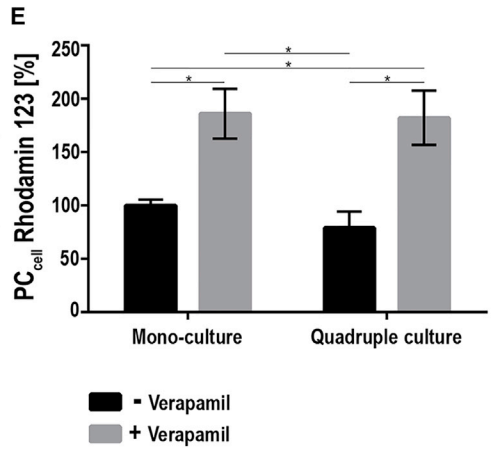

Figure 3. Establishment of BBB Transwell Models, Tightness Characterization, Gene Expression, and Transporter Functionality

(A) Schematic overview of BBB model establishment in transwell systems. At day −1, in total 5 × 10^4 co-culture cells were seeded in the basolateral compartment. At day 0, 1 × 10^6 hiPS-ECs/cm^2 were seeded on collagen IV-/fibronectin-coated transwell membranes (no direct

(legend continued on next page)

Table 1. Overview of the Results of the Permeability Studies with Paracellular Marker Molecules

	PC_{all} (μm/min)	PC_{cell} (μm/min)	Transport Ranking
Mono-culture			
Lucifer yellow	1.41 ± 0.25	1.52 ± 0.29	1
Fluorescein	1.39 ± 0.59	1.53 ± 0.67	1
FITC-labeled dextran 4 kDa	0.0166 ± 0.0037	0.0166 ± 0.0037	3
FITC-labeled dextran 40 kDa	0.0054 ± 0.0007	0.0054 ± 0.0007	4
Quadruple Culture			
Lucifer yellow	1.44 ± 0.34	1.58 ± 0.40	1
Fluorescein	1.26 ± 0.27	1.33 ± 0.29	2
FITC-labeled dextran 4 kDa	0.0106 ± 0.0016	0.0106 ± 0.0016	3
FITC-labeled dextran 40 kDa	0.0030 ± 0.0004*	0.0030 ± 0.0004*	4

Data are presented as means ± SEM, n = 6–8 from three to four independent experiments. Statistically significant difference, *p < 0.05, in comparison with the mono-culture setup. PC, permeability coefficient.
Permeability coefficients and transport rankings are compared between mono- and quadruple culture models.

further analyses focused on the comparison between the mono-culture and the quadruple setup. To characterize the functionality of the efflux transporter P-glycoprotein, we performed transport studies with the substrate rhodamine 123 with and without inhibiting the transporter by use of verapamil (Figure 3E). The permeability coefficients (PC_{cell}) for rhodamine 123 could be significantly increased in the mono-culture setup as well as in the quadruple culture by adding verapamil, indicating the correct transporter functionality and polarization in the cell membrane.

To characterize the paracellular permeability of the cell layers in a molecular size-dependent manner, transport studies with several paracellular marker molecules such as lucifer yellow (~0.44 kDa), fluorescein (~0.33 kDa), and FITC-labeled dextrans (4 and 40 kDa) were accomplished (Table 1). As expected, lucifer yellow and fluorescein permeated very similarly (PC_{cell} ~1.5 μm/min). FITC-labeled dextran (4 kDa) migrated about 100-fold slower than these two small paracellular markers, and the PCs for 40 kDa FITC-labeled dextran were even smaller (PC_{cell} 0.003–0.0054 μm/min). Corresponding to the TEER values, comparison with the mono-culture revealed a lower, statistically significant different permeability of 40 kDa FITC-labeled dextran across the quadruple cultures.

Paracellular permeability is functionally linked to the expression of junctional molecules, especially of claudins (*CLDN*). Therefore, the expression of major TJ and TJ-associated molecules was analyzed. In addition to occludin (*OCLN*, Figure 3D), we determined mRNA expression of *CLDN3*, *CLDN4*, *CDH5*, and *TJP1* (ZO-1) of quadruple cultures in direct comparison with mono-cultures, however upregulation was mostly below the threshold of 1.5-fold, and no statistical significant effects were detected (data not shown). The expression of all analyzed genes could be qualitatively confirmed representatively in mono-cultures by gel electrophoresis of PCR products (Figure S2). At the protein level, the presence of the TJ proteins CLDN1, CLDN4, and CLDN5 was also confirmed, again without any statistically significant change in

contact with co-culture cells). At day 1, the growth factor concentration in the growth medium was reduced to stop hiPS-EC proliferation. The models were analyzed at day 2 by TEER measurement, qRT-PCR, western blot, electron microscopy, and transport studies.
(B) Ten different variants of BBB models were established as transwell systems to investigate the impact of different co-culture cells on BBB integrity. TEER was measured at day 2 of co-culture and compared with hiPS-EC mono-culture models. TEER was most significantly increased by triple culture of hiPS-ECs with hiPS-NSCs and pericytes as well as by quadruple cultivation, indicated by the red box. Absolute TEER values are presented as means ± SD after data block-wise correction (n = 4); each biological replicate represents a new differentiation (**p < 0.01).
(C) Overview of the minimal as well as the maximal measured TEER values of all ten variants of BBB models, representing the variabilities across the four independent biological experiments. Absolute TEER values are represented as measured raw data without manual data block-wise correction.
(D) qRT-PCR analyses of efflux transporter *ABCB1*, glutamate transporter *SLC1A1*, glucose transporter *SLC2A1*, and occludin *OCLN* in hiPS-ECs of different co-culture BBB models shown as the change in gene expression compared with the hiPS-EC mono-culture model. Results are shown as means ± SD (n = 3–10); each biological replicate represents a new differentiation and co-culture experiment. Housekeeping genes for normalization were *EEF1A1* and *RPL6*. The black horizontal line indicates an arbitrary threshold of 1.5-fold increase (***p < 0.001).
(E) Permeability coefficients of the hiPS-ECs (PC_{cell}) after 15 min of transport of 100 μM rhodamine 123 compared between mono-cultures and quadruple cultures with and without 100 μM verapamil treatment. Results are shown as means ± SEM (n = 4–6); each biological replicate represents a new differentiation and co-culture experiment (*p < 0.05).

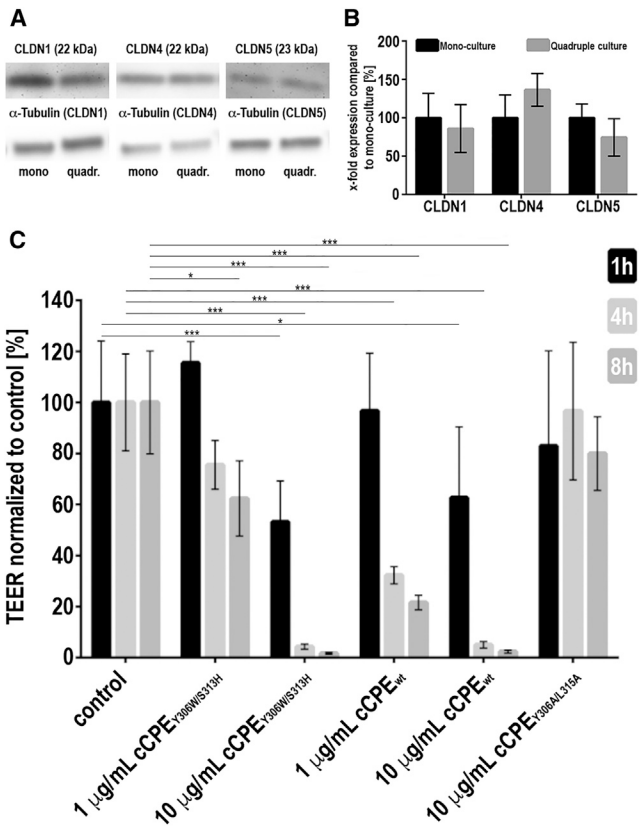

Figure 4. Expression of Major Tight Junction Proteins and Relevance of Claudins for Barrier Tightness

(A) Western blot analysis of the TJ proteins (upper line) CLDN1 (22 kDa), CLDN4 (22 kDa), and CLDN5 (23 kDa) compared with mono-cultures (left lanes) and quadruple cultures (right lanes). α-Tubulin 52 kDa (lower line) was used in all blots as loading control. See also Figure S2 for further details.

(B) Quantitative analysis of western blot results of the TJ proteins CLDN1, CLDN4, and CLDN5 shown as the change in protein expression compared with the hiPS-EC mono-culture models and hiPS-ECs of the quadruple cultures.

(C) Effects of $cCPE_{Y306W/S313H}$, $cCPE_{wt}$, $cCPE_{Y306A/L315A}$ proteins on TEER progression (%) of hiPSC-derived BBB monolayers normalized to the progression of controls. $cCPE_{wt}$ binds with high affinity to CLDN3/4 and interacts with CLDN1, whereas $cCPE_{Y306W/S313H}$ interacts strongly with CLDN5. The $cCPE_{Y306A/L315A}$ control does not bind to claudins. Data are presented as means ± SD (n = 3–6); independent biological replicates (*p < 0.05, ***p < 0.001).

expression as shown by western blot analysis (Figures 4A and 4B).

In order to confirm the role of claudins for paracellular tightness from BBB hiPS-EC layers, the effects of claudin-specific TJ modulators on TEER were investigated (Figure 4C). These TJ modulators were based on the claudin-binding domain of the *Clostridium perfringens* enterotoxin (Protze et al., 2015). Data revealed a significant time- and concentration-dependent decrease of TEER after addition of $cCPE_{wt}$, which binds with high affinity to CLDN3/4 and interacts with CLDN1. Furthermore, incubation with CLDN5-binding $cCPE_{Y306W/S313H}$ decreased TEER. On the contrary, application of the non-binding control $cCPE_{Y306A/L315A}$ showed no effects on TEER progression. Interestingly, 1 µg/mL $cCPE_{wt}$ reduced TEER to 32% ± 3% after 4 hr, whereas 1 µg/mL $cCPE_{Y306W/S313H}$ (76% ± 10%) did not significantly disrupt the barrier. Since cCPE_Y306W/S313H has a higher affinity for CLDN5 than cCPE_wt (K_d ~30 nM versus $K_d \gg 1$ µM; Protze et al., 2015), the results indicated that, in our model, other claudins next to claudin-5 contribute strongly to the high TEER values and formation of the paracellular barrier.

Freeze-Fracture and Transmission Electron Microscopy

To characterize the TJs on the ultrastructural level, cells were fixed, and freeze-fracture electron microscopy (EM) was performed. Intramembranous TJ particles were found on the protoplasmic face (P face, PF) and exoplasmic face (E face, EF) of the plasma membrane (Figure 5). On the E face, TJ strands were detected as particles and particle-free grooves. On the P face, TJ strands were detected partly as continuous strands and partly as beaded particles (Figure 5). Quadruple cultures and mono-cultures showed variable although similar complex networks of meshes formed by branched strands with mixed P/E face association. A tendency to higher complexity was found for the quadruple cultures (mean number of meshes in the strand network, 33.0 ± 5.0 versus 26.1 ± 2.8; rectangular area with strands, 1.1 ± 0.1 μm^2 versus 0.9 ± 0.1 μm^2; mesh density, 33.4 ± 2.7 μm^{-2} versus 30.6 ± 2.8 μm^{-2}; n > 20). However, no significant differences were obtained for any of these morphometric parameters. In sum, on the ultrastructural level, for BBB hiPS-ECs, TJs similar to those of brain capillary ECs of the BBB were found (Wolburg et al., 1994).

Transmission EM also revealed the presence of complex TJs, constricting the paracellular gap and connecting two neighboring hiPS-ECs (Figures 5E–5G). However, no significant differences of TJs between mono- and quadruple culture models were found.

Drug Transport Studies

In addition to the restriction of paracellular permeability, the BBB is also a barrier for transcellular transport. To describe these properties and to perform a first assessment about the qualification for drug transport studies, permeation of several reference drugs was studied across the mono-culture and quadruple culture setup. Calculated PCs across the total barrier comprising the cell layer and the membrane support (PC_{all}) revealed mean permeabilities from 3.44 to 26.94 µm/min (Table 2). Especially in the case of transport studies of compounds migrating via

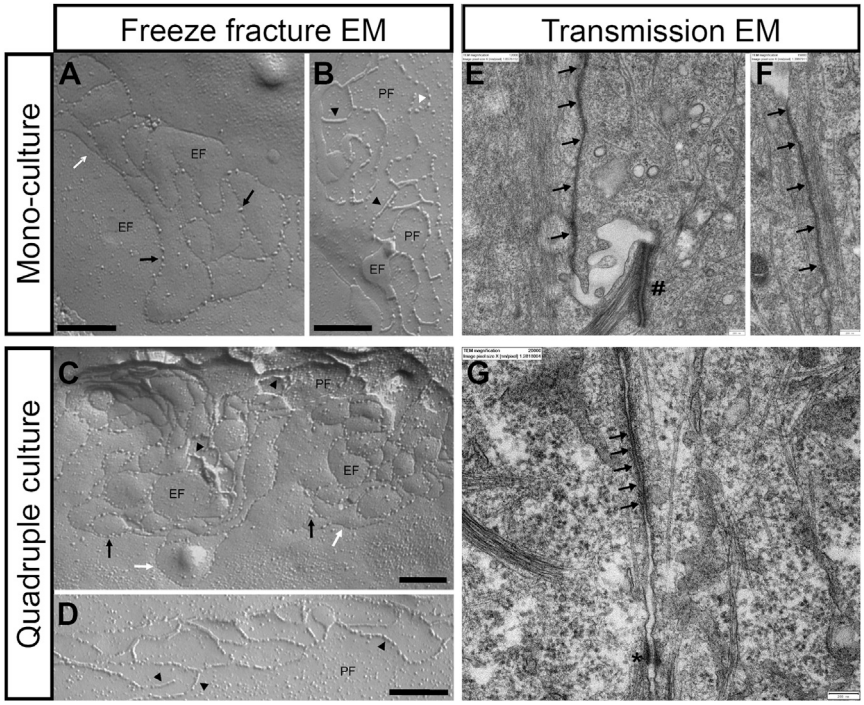

Figure 5. Ultrastructural Analysis of BBB Mono-culture and Quadruple Culture Models

(A–D) Freeze-fracture EM analysis of the TJ ultrastructure of hiPS-ECs cultured without (A and B) or with (C and D) co-culture cells. Similar to brain microcapillary ECs in vivo, intramembranous TJ particles were found on the protoplasmic face (P face, PF) and exoplasmic face (E face, EF) of the plasma membrane. On the E face, TJ strands were detected as particles (black arrows) and particle-free grooves (white arrows). On the P face, TJ strands were detected as continuous strands (black arrowheads) and as beaded particles (white arrowheads). Mono-cultures (A and B) and quadruple cultures (C and D) showed variable although similar complex networks of meshes formed by branched strands with mixed P/E face association. Scale bars, 200 nm.

(E–G) Transmission EM micrographs of the BBB models. Neighboring hiPS-ECs of both mono-cultures (E and F) and quadruple cultures (G) are connected by complex TJs constricting the paracellular space (black arrows). Furthermore, large desmosomes (macula adherens, black hash in E) anchored with intermediate filaments were detected as well as adhesion points (punctum adherens, black asterisk in G) anchored within the actin filament network. Scale bars, 200 nm.

the transcellular route, correction of the PC for the barrier formed by the membrane support itself is essential to obtain the permeability only across the cell layer (PC_{cell}). This correction procedure revealed significantly increased PCs. In addition to accounting for cell layer variabilities, diazepam was used as an internal standard for each compound, and the permeability rankings were calculated with the PC_{cell} data normalized to the PC_{cell} data of diazepam. These rankings showed that diazepam permeated fastest followed by caffeine, ibuprofen, celecoxib, diclofenac, loratadine, and rhodamine 123 across the mono-culture model. This ranking was according to the classification based on literature data for diazepam and caffeine as fast, ibuprofen, celecoxib, and diclofenac as medium, and loratadine and rhodamine 123 as slow permeating compounds (Nakazono et al., 1992; Neuhaus et al., 2012; Novakova et al., 2014). In the case of the quadruple culture, the mean ratio to diazepam was significantly decreased for caffeine, from 0.499 to 0.251, leading to a switch in the ranking position from second to fourth place in comparison with the mono-culture setup.

DISCUSSION

In order to closely mimic the BBB in vivo and to optimize model characteristics, we analyzed a set of different BBB co-culture models based on primary cells (astrocytes, pericytes, and NSCs) and hiPSC-derived cells (hiPS-ECs, hiPS-NSCs, and hiPS-As). Compared with all existing BBB models, in vivo-like TEER values of up to 3,600 Ω cm^2 could only been achieved by use of hiPS-ECs (Lippmann et al., 2012, 2014). To a similar extent, this could also be confirmed with our current study using the same hiPSC line IMR90-4 and different co-culture settings. In comparison, for the hCMEC/D3 human reference BBB cell line, TEER levels lower than 40 Ω cm^2 were reported (Weksler et al., 2005), which could be strongly increased by dynamic flow culture conditions at best (Cucullo et al., 2008), but this still does not represent in vivo conditions.

In previous hiPSC studies, hiPS-ECs with specific BBB characteristics, such as the expression of BBB-relevant TJ proteins and transporter molecules, were generated by a co-culture of hiPS-ECs with a mixture of neural cells and astrocytes (Lippmann et al., 2014). Similarly, we also included NSCs isolated from fetal human brain tissue or differentiated from hiPSCs. Besides neural cells, astrocytes and pericytes are also important BBB niche cells, which seem to have beneficial effects on barrier integrity and transporter expression in vitro (Lim et al., 2007; Al Ahmad et al., 2011; Lippmann et al., 2012). In our studies, we used primary brain-derived astrocytes and pericytes of human origin as reference cells in order to stay species consistent.

Table 2. Overview of the Results of the Transport Studies

	Substance		Diazepam			Transport Ranking
	PC_{all} (μm/min)	PC_{cell} (μm/min)	PC_{all} (μm/min)	PC_{cell} (μm/min)	Ratio to Diazepam	
Mono-culture						
Diazepam	21.58 ± 0.56[a]	250.06 ± 31.31[a]			1 ± 0.0	1
Caffeine	15.15 ± 1.73	51.06 ± 9.90	20.52 ± 1.42	103.36 ± 19.83	0.499 ± 0.043	2
Ibuprofen	17.19 ± 0.89	90.33 ± 14.51	22.25 ± 0.76	377.44 ± 91.69	0.281 ± 0.043	3
Celecoxib	16.21 ± 0.26	42.15 ± 1.82	19.73 ± 0.61	201.81 ± 36.34	0.259 ± 0.060	4
Diclofenac	13.17 ± 0.34	39.98 ± 4.33	22.21 ± 0.45	199.49 ± 39.14	0.224 ± 0.026	5
Loratadine	3.44 ± 0.46	5.78 ± 0.83	18.12 ± 0.83	259.56 ± 118.36	0.036 ± 0.010	6
Rhodamine 123	7.11 ± 2.38	7.44 ± 2.57	26.94 ± 1.09	354.38 ± 84.66	0.024 ± 0.009	7
Quadruple Culture						
Diazepam	21.56 ± 0.57[a]	229.57 ± 24.74[a]			1 ± 0.0	1
Caffeine	13.32 ± 1.31	34.44 ± 4.40	22.16 ± 1.90	146.74 ± 27.03	0.251 ± 0.046*	4
Ibuprofen	17.20 ± 0.73	86.30 ± 10.18	22.28 ± 0.50	303.67 ± 42.84	0.295 ± 0.032	2
Celecoxib	15.51 ± 0.72	38.98 ± 4.33	18.96 ± 0.93	190.59 ± 60.12	0.296 ± 0.064	2
Diclofenac	13.22 ± 0.39	41.23 ± 5.67	22.17 ± 0.63	227.99 ± 70.30	0.227 ± 0.036	5
Loratadine	3.80 ± 0.52	6.83 ± 0.94	18.28 ± 0.62	202.72 ± 60.81	0.040 ± 0.008	6
Rhodamine 123	4.83 ± 1.47	4.97 ± 1.55	26.17 ± 1.17	288.91 ± 82.16	0.022 ± 0.007	7

Data are presented as means ± SEM, n = 4–6 from three independent experiments. Ratio to diazepam: PC_{cell} value of the substance divided by the PC_{cell} value of diazepam for each single cell layer; this may lead to differences compared with merely dividing the average PC_{cell} values of the substance by the value for diazepam. Statistically significant difference, *$p < 0.05$, in comparison with the ratio in the mono-culture setup. PC, permeability coefficient. Permeability coefficients: ratios to diazepam and transport rankings are compared between mono-culture and quadruple culture models.

[a]Transport studies were accomplished with the investigated substance and the internal standard diazepam at the same time; for comparison reasons, the total average PC values of diazepam of all mono-culture or quadruple culture studies are presented (n = 30).

Furthermore, we have applied recent protocols for NSC and subsequent astrocyte generation from hiPSCs (Reinhardt et al., 2013; Yan et al., 2013). The advantage of all these protocols lay in the inexhaustible, rapid, and reliable differentiation of pluripotent stem cells as adherent 2D cultures, avoiding embryoid body formation and the tendency of spontaneous cell dedifferentiation (Conti and Cattaneo, 2010).

Taken together, by use of our established, well-standardized protocols, we were able to differentiate hiPSCs into hiPS-ECs with BBB characteristics within 12 days, hiPS-NSCs within 1 week, as well as multipotent NSCs into astrocytes in only 30 days. We demonstrated the pluripotency of hiPSCs as well as the multipotency of NSCs by expression of characteristic markers; this was in line with previous studies (Yu et al., 2007; Yan et al., 2013; Chen et al., 2015). All further differentiated cells showed specific sets of markers at the protein as well as gene expression level.

Our study describes the systematic combination of various cell types in different complex co-culture setups to investigate the influence on hiPS-ECs regarding TEER, expression of BBB-relevant genes, and transport of specific substrates. Indeed, the most robust BBB properties could be achieved by the quadruple culture of BBB ECs with hiPS-NSCs, primary astrocytes, and pericytes, which is in line with previous studies (Lippmann et al., 2013, 2014; Cecchelli et al., 2014). In contrast to these reports, the BBB models in our study were established with constant seeding densities of co-culture cells allowing us to compare the direct biological impact on hiPS-ECs. Moreover, instead of sequentially applied co-cultures, we analyzed the simultaneous co-culture effects to reflect complex cell-cell interactions and the in vivo-like conditions. Thus, the tightness and expression of BBB-relevant genes in the quadruple culture was significantly increased. Noteworthy, altered TEER did not correspond with specific upregulation of TJ-associated genes, which confirms recent data from the Shusta group (Canfield et al., 2016).

The paracellular barrier against small ions and molecules in hiPS-EC cultures formed by TJs were functionally

detected by high TEER and low flux of paracellular marker molecules. On the ultrastructural level, the presence of TJs was clearly demonstrated by freeze-fracture EM as well as transmission EM. The TJs appeared to be similar to those reported earlier for other hiPS-ECs (Lippmann et al., 2012). Furthermore, we found complex networks of meshes formed by branched TJ strands, which at least partly correlates with barrier properties (Claude, 1978) and are comparable with those of brain ECs in vivo (Wolburg et al., 1994; Kniesel et al., 1996). Also similar to the BBB, in vivo intramembranous TJ particles were strongly associated with the P face, a parameter that correlates with tightness of the barrier. In general, tight brain capillary ECs form TJs with a characteristic mixed P/E face association with more than 50% of the TJ particles on the P face (Wolburg et al., 1994; Kniesel et al., 1996). It was shown that the ultrastructure of TJs including the P/E face association is at least partly dependent on the CLDN composition (Liebner et al., 2000) and CLDN subtype-specific interactions. Hence, the mixed P/E face association found for hiPS-EC cultures fits with the expression of CLDN5 together with CLDN1, 3, or 4 (Furuse et al., 1999; Piontek et al., 2011).

These ultrastructural findings were also consistent with TEER experiments and cCPE-based claudin-binding TJ modulators, showing that several claudins were probably responsible for high TEER values in our hiPSC-derived BBB model (Protze et al., 2015). All the claudins found to be expressed in hiPS-ECs were reported to be potentially expressed in the BBB (Kratzer et al., 2012). In sum, the data presented in this study suggest the quadruple culture as an in vitro BBB model with in vivo-like TJ characteristics.

In addition to the comprehensive characterization of the paracellular barrier of our models, transport studies with small molecules known for permeating via the transcellular route were accomplished. According to the literature, diazepam permeated fastest, followed by caffeine, ibuprofen, celecoxib, diclofenac, loratadine, and rhodamine 123 in the mono-culture setup. In in vitro tests, caffeine, a more hydrophilic compound, was shown to permeate almost as fast as diazepam, a lipophilic compound often used as a fast-migrating transcellular marker that does not interact with efflux transporters (Zhao and Pollack, 2009; Mealey et al., 2010). On the contrary, in vivo data revealed that caffeine was significantly slower than diazepam, probably due to interactions with active transporters (Nakazono et al., 1992; Yusof et al., 2014). These in vivo observations were also reflected in our models. Moreover, transport of caffeine was significantly further decreased in the quadruple culture compared with the mono-culture, indicating an even more in vivo-like phenotype in the quadruple culture. In concordance with in vitro data obtained from BBB models based on rat primary cells, ibuprofen was also faster than diclofenac in our models (Novakova et al., 2014). Loratadine and rhodamine 123 are known to be strong substrates of the efflux pump P-glycoprotein and to permeate significantly slower than diazepam (Obradovic et al., 2007; Neuhaus et al., 2012). This was also found in our models. However, it is important to point out that the slowest compounds, loratadine and rhodamine 123, were still significantly faster than the paracellular markers fluorescein or lucifer yellow in our models (PC_{cell} 5–8 μm/min versus ~1.5 μm/min). Lippmann et al. (2012) published a dynamic range of PCs with about 40-fold between diazepam and sucrose; in our models, a 150-fold difference was achieved comparing PC_{cell} values from diazepam to fluorescein. However, in this case, it is important to mention that Lippmann et al. (2012) did not include blank values in their calculation procedure, used another transport study design (sampling versus transferring) as well as other transport buffer compositions, and probably applied different substance concentrations. Considering these variables, the published PC of diazepam (11 μm/min) was in a similar range to the PC_{all} values for diazepam in our studies (18–27 μm/min). With regard to the paracellular tightness, PCs for low-molecular-weight markers such as sucrose (0.342 kDa) of high-fidelity BBB animal in vitro models were between 0.1 and 1 μm/min, which was also in a similar range to our models (Perriere et al., 2007; Malina et al., 2009). Moreover, the quadruple model revealed an average PC of 0.0106 μm/min for FITC-labeled dextran 4 kDa and 0.0030 μm/min for FITC-labeled dextran 40 kDa. In comparison with these data, the standard human BBB cell line hCMEC/D3 formed significantly leakier cell layers (fluorescein, 55 μm/min; FITC-labeled dextran 4 kDa, 8.3 μm/min) (Forster et al., 2008). Taken together, compared with the mono-culture, the quadruple culture provides a model with significantly higher barrier integrity and altered transcellular drug transport. For substances whose transport is significantly affected by drug transporters (influx or efflux), a tight human model could be preferential. In terms of BBB-specific gene abundance, we saw only moderate effects, suggesting that protein organization and localization might be much more influenced by the co-culture and causative for altered BBB function. Consequently, methods to evaluate BBB model integrity might indeed include non-invasive TEER measurement, permeation studies with paracellular markers, and estimation of BBB transporter activity.

In future experiments, long-term cultures of BBB models could be of interest, offered potentially by the use of dynamic flow culture conditions, to further study chronic diseases such as Alzheimer's disease and Parkinson's disease. In this respect, there is increasing interest in so-called organ-on-a-chip technologies, which will allow the study of complex organ interaction, e.g., of the BBB and liver, under dynamic flow conditions. Furthermore, based on recent

differentiation protocols for hiPSC-derived astrocytes and pericytes, our approach could be further developed to establish fully isogenic BBB models (Orlova et al., 2014; Canfield et al., 2016). With these protocols in hand, isogenic cultures will be possible in future applications. Finally, by working with patient-specific cells, reprogrammed to pluripotent stem cells, BBB models from one individual donor could be established, which might lead to more effective personalized therapies or novel drugs (Grskovic et al., 2011; Okano and Yamanaka, 2014).

EXPERIMENTAL PROCEDURES

Co-culture Experiments in Transwell Settings

To investigate the influence of different co-culture setups on BBB EC integrity, the same cell density of 5 × 10^4 cells per cm^2 was seeded in 24-well plates (Sigma-Aldrich) in all experiments. Plate coating depended on individual co-culture cell type: astrocytes, pericytes, and combinations of both were cultured on 10 μg/mL poly-L-lysine (PELOBiotech); hiPS-NSCs and fNSCs as well as all respective combinations on 15 μg/mL poly-L-ornithine (Sigma-Aldrich) + 1 μg/mL laminin (Sigma-Aldrich); and hiPSC-As on Matrigel (BD Biosciences; 1:100 in DMEM/F-12, Life Technologies). Seeding was performed 24 hr prior to co-culture with BBB hiPS-ECs; seeding density is described in Table S1.

NSCs from fetal brain tissue were isolated after induced abortions between the 11^{th} and 12^{th} weeks of pregnancy. Informed consent was obtained beforehand, and the study was approved by the local ethics committee of the Julius-Maximilians-University Würzburg (reference number 151/14).

After 24 hr of pre-culture, BBB hiPS-ECs were sub-cultured on collagen IV-coated (Sigma-Aldrich) and fibronectin-coated (Life Technologies) 24-well inserts (Sigma-Aldrich) and maintained for 24 hr as a mono- or co-culture in EC medium + hbFGF + RA (human Endothelial-SFM [Life Technologies] supplemented with 1% platelet-poor plasma-derived bovine serum [Alfa Aesar], 20 ng/mL hbFGF [PeproTech], and 10 μM all-*trans* RA [Sigma-Aldrich]). Thereafter, cultures were continued and combined with a 24-hr treatment with EC medium (without hbFGF and RA). Detailed information on coating preparation and medium composition is given in the Supplemental Information.

Transport Studies

Transport assays were performed in 24-well transwells under serum-free conditions on a rocking shaker KM-2 AKKU (Edmund Bühler) at 100 rpm, 37°C, 95% humidity, and 5% CO_2. All substances were dissolved at their specific concentrations (see Table S2) in human Endothelial-SFM. In the case of FITC-labeled dextrans, the dissolved stock solutions were purified from residual-free FITC before use by ultrafiltration using Amicon 3 kDa filter tubes (Millipore). The test substance (200 μL) was pipetted on the apical (top) side of the BBB models. The basolateral (bottom) side was supplied with 800 μL of pure human Endothelial-SFM. Every 15 min, inserts were transferred into new pre-warmed wells filled with 800 μL of pure human Endothelial-SFM. Incubation times for FITC-labeled dextran reference compounds were 0.5 hr, 1.5 hr, 3.5 hr, 7.5 hr, and 30.5 hr. The transport assay was stopped after 60 min (FITC-labeled dextran, 30.5 hr). Transporter inhibition experiments with verapamil were performed for 15 min; to block the function of P-glycoprotein, rhodamine 123 and verapamil had to be combined to their final concentrations. Transport in quadruple culture models and hiPS-EC mono-cultures were compared. As control, all substances were also incubated on empty collagen IV-/fibronectin-coated inserts. For comparison reasons, transport assays were performed without the co-cultures to prevent drug absorption by these cells. All permeability studies were performed in duplicate and three independent biological replicates. Supernatants of samples, which were precipitated with acetonitrile (VWR) (1:2) at 4°C for 60 min and centrifuged at 12,000 rpm for 10 min, were analyzed by high-performance liquid chromatography (HPLC) (detailed method description, see Table S3). Peak areas were used to calculate PCs. PC_{all} and PC_{cell} following the clearance principle as previously published (Novakova et al., 2014).

Statistical Analysis

All experiments were performed at least three times. The level of statistical significance was set at $p < 0.05$, indicated with an asterisk (*). Detailed information about the individual statistical tests applied can be found in the Supplemental Information.

SUPPLEMENTAL INFORMATION

Supplemental Information includes Supplemental Experimental Procedures, two figures, and five tables and can be found with this article online at http://dx.doi.org/10.1016/j.stemcr.2017.02.021.

AUTHOR CONTRIBUTIONS

A.A.-M., H.W., W.N., and M.M. conceived the study. A.A.-M. and A.C. performed all cell-culture experiments and related analyses. W.N. analyzed the samples of the transport studies via HPLC and accomplished the protein construct TEER studies. K.G. and F.E. performed and validated NSC differentiation from hiPSCs and contributed to iPSC validation. J.P. analyzed the ultrastructure of the TJ networks. All authors contributed to manuscript preparation. Essential tissue was provided by T.S.

ACKNOWLEDGMENTS

We would like to thank Dr. Georg Krohne (University Würzburg) for transmission EM, Sabine Wilhelm and Martina Werner (University Hospital Würzburg) for the western blot analysis, Sarah Frosch (University Hospital Würzburg) for qRT-PCR, In-Fah MLee (Charité Berlin) for conducting freeze-fracture EM and Dr. Anna Piontek (Leibniz Inst. f. Mol. Pharmak.) for preparation of GST-cCPE fusion proteins. We are grateful to the Department of Pharmaceutical Chemistry, University of Vienna, for providing access to the HPLC and cellZscope devices. This work was supported by public funding from the German Ministry for Education and Research BMBF (LipoTrans, funding code: 13N11803), the German Research Foundation (DFG ED79/4-1 to F.E.), and the SET foundation (Stiftung zur Förderung der Erforschung von Ersatz- und Ergänzungsmethoden zur Einschränkung von Tierversuchen, project 060 to W.N. and M.M.).

Received: April 8, 2016
Revised: February 22, 2017
Accepted: February 23, 2017
Published: March 23, 2017

REFERENCES

Al Ahmad, A., Taboada, C.B., Gassmann, M., and Ogunshola, O.O. (2011). Astrocytes and pericytes differentially modulate blood-brain barrier characteristics during development and hypoxic insult. J. Cereb. Blood Flow Metab. *31*, 693–705.

Avdeef, A., Deli, M.A., and Neuhaus, W. (2015). In Vitro Assays for Assessing BBB Permeability. Blood-brain Barrier in Drug Discovery (John Wiley), pp. 188–237.

Boyer-Di Ponio, J., El-Ayoubi, F., Glacial, F., Ganeshamoorthy, K., Driancourt, C., Godet, M., Perriere, N., Guillevic, O., Couraud, P.O., and Uzan, G. (2014). Instruction of circulating endothelial progenitors in vitro towards specialized blood-brain barrier and arterial phenotypes. PLoS One *9*, e84179.

Butt, A.M., Jones, H.C., and Abbott, N.J. (1990). Electrical resistance across the blood-brain barrier in anaesthetized rats: a developmental study. J. Physiol. *429*, 47–62.

Canfield, S.G., Stebbins, M.J., Morales, B.S., Asai, S.W., Vatine, G.D., Svendsen, C.N., Palecek, S.P., and Shusta, E.V. (2016). An isogenic blood-brain barrier model comprising brain endothelial cells, astrocytes and neurons derived from human induced pluripotent stem cells. J. Neurochem http://dx.doi.org/10.1111/jnc.13923.

Cecchelli, R., Berezowski, V., Lundquist, S., Culot, M., Renftel, M., Dehouck, M.P., and Fenart, L. (2007). Modelling of the blood-brain barrier in drug discovery and development. Nat. Rev. Drug Discov. *6* (8), 650–661.

Cecchelli, R., Aday, S., Sevin, E., Almeida, C., Culot, M., Dehouck, L., Coisne, C., Engelhardt, B., Dehouck, M.P., and Ferreira, L. (2014). A stable and reproducible human blood-brain barrier model derived from hematopoietic stem cells. PLoS One *9*, e99733.

Chen, W., Huang, J., Yu, X., Lin, X., and Dai, Y. (2015). Generation of induced pluripotent stem cells from renal tubular cells of a patient with Alport syndrome. Int. J. Nephrol. Renovasc. Dis. *8*, 101–109.

Claude, P. (1978). Morphological factors influencing transepithelial permeability: a model for the resistance of the zonula occludens. J. Membr. Biol. *39* (2-3), 219–232.

Conti, L., and Cattaneo, E. (2010). Neural stem cell systems: physiological players or in vitro entities? Nat. Rev. Neurosci. *11* (3), 176–187.

Crone, C., and Olesen, S.P. (1982). Electrical resistance of brain microvascular endothelium. Brain Res. *241*, 49–55.

Cucullo, L., Couraud, P.O., Weksler, B., Romero, I.A., Hossain, M., Rapp, E., and Janigro, D. (2008). Immortalized human brain endothelial cells and flow-based vascular modeling: a marriage of convenience for rational neurovascular studies. J. Cereb. Blood Flow Metab. *28*, 312–328.

Deli, M.A., Abraham, C.S., Kataoka, Y., and Niwa, M. (2005). Permeability studies on in vitro blood-brain barrier models: physiology, pathology, and pharmacology. Cell Mol. Neurobiol. *25*, 59–127.

Eigenmann, D.E., Xue, G., Kim, K.S., Moses, A.V., Hamburger, M., and Oufir, M. (2013). Comparative study of four immortalized human brain capillary endothelial cell lines, hCMEC/D3, hBMEC, TY10, and BB19, and optimization of culture conditions, for an in vitro blood-brain barrier model for drug permeability studies. Fluids Barriers CNS *10*, 33.

Forster, C., Burek, M., Romero, I.A., Weksler, B., Couraud, P.O., and Drenckbahni, D. (2008). Differential effects of hydrocortisone and TNF alpha on tight junction proteins in an in vitro model of the human blood-brain barrier. J. Physiol. *586*, 1937–1949.

Furuse, M., Sasaki, H., and Tsukita, S. (1999). Manner of interaction of heterogeneous claudin species within and between tight junction strands. J. Cell Biol. *147*, 891–903.

Gaillard, P.J., and de Boer, A.G. (2000). Relationship between permeability status of the blood-brain barrier and in vitro permeability coefficient of a drug. Eur. J. Pharm. Sci. *12*, 95–102.

Grskovic, M., Javaherian, A., Strulovici, B., and Daley, G.Q. (2011). Induced pluripotent stem cells–opportunities for disease modelling and drug discovery. Nat. Rev. Drug Discov. *10*, 915–929.

Günther, K., Appelt-Menzel, A., Keong Kwok, C., Walles, H., Metzger, M., and Edenhofer, F. (2016). Rapid monolayer neural induction of induced pluripotent stem cells yields stably proliferating neural stem cells. J. Stem Cell Res. Ther. *6*, 6.

Hawkins, B.T., and Davis, T.P. (2005). The blood-brain barrier/neurovascular unit in health and disease. Pharmacol. Rev. *57*, 173–185.

Kadari, A., Lu, M., Li, M., Sekaran, T., Thummer, R.P., Guyette, N., Chu, V., and Edenhofer, F. (2014). Excision of viral reprogramming cassettes by Cre protein transduction enables rapid, robust and efficient derivation of transgene-free human induced pluripotent stem cells. Stem Cell Res. Ther. *5*, 47.

Kniesel, U., Risau, W., and Wolburg, H. (1996). Development of blood-brain barrier tight junctions in the rat cortex. Brain Res. Dev. Brain Res. *96*, 229–240.

Kratzer, I., Vasiljevic, A., Rey, C., Fevre-Montange, M., Saunders, N., Strazielle, N., and Ghersi-Egea, J.F. (2012). Complexity and developmental changes in the expression pattern of claudins at the blood-CSF barrier. Histochem. Cell Biol. *138*, 861–879.

Liebner, S., Kniesel, U., Kalbacher, H., and Wolburg, H. (2000). Correlation of tight junction morphology with the expression of tight junction proteins in blood-brain barrier endothelial cells. Eur. J. Cell Biol. *79*, 707–717.

Lim, J.C., Wolpaw, A.J., Caldwell, M.A., Hladky, S.B., and Barrand, M.A. (2007). Neural precursor cell influences on blood-brain barrier characteristics in rat brain endothelial cells. Brain Res. *1159*, 67–76.

Lippmann, E.S., Azarin, S.M., Kay, J.E., Nessler, R.A., Wilson, H.K., Al-Ahmad, A., Palecek, S.P., and Shusta, E.V. (2012). Derivation of blood-brain barrier endothelial cells from human pluripotent stem cells. Nat. Biotechnol. *30*, 783–791.

Lippmann, E.S., Al-Ahmad, A., Palecek, S.P., and Shusta, E.V. (2013). Modeling the blood-brain barrier using stem cell sources. Fluids Barriers CNS *10*, 2.

Lippmann, E.S., Al-Ahmad, A., Azarin, S.M., Palecek, S.P., and Shusta, E.V. (2014). A retinoic acid-enhanced, multicellular human blood-brain barrier model derived from stem cell sources. Sci. Rep. *4*, 4160.

Malina, K.C.K., Cooper, I., and Teichberg, V.I. (2009). Closing the gap between the in-vivo and in-vitro blood-brain barrier tightness. Brain Res. *1284*, 12–21.

Mealey, K.L., Waiting, D., Raunig, D.L., Schmidt, K.R., and Nelson, F.R. (2010). Oral bioavailability of P-glycoprotein substrate drugs do not differ between ABCB1-1Delta and ABCB1 wild type dogs. J. Vet. Pharmacol. Ther. *33*, 453–460.

Nakazono, T., Murakami, T., Sakai, S., Higashi, Y., and Yata, N. (1992). Application of microdialysis for study of caffeine distribution into brain and cerebrospinal fluid in rats. Chem. Pharm. Bull. (Tokyo) *40*, 2510–2515.

Neuhaus, W., and Noe, C.R. (2010). Transport at the Blood–brain Barrier Transporters as Drug Carriers (Wiley-VCH Verlag), pp. 263–298.

Neuhaus, W., Mandikova, J., Pawlowitsch, R., Linz, B., Bennani-Baiti, B., Lauer, R., Lachmann, B., and Noe, C.R. (2012). Blood-brain barrier in vitro models as tools in drug discovery: assessment of the transport ranking of antihistaminic drugs. Pharmazie *67*, 432–439.

Novakova, I., Subileau, E.A., Toegel, S., Gruber, D., Lachmann, B., Urban, E., Chesne, C., Noe, C.R., and Neuhaus, W. (2014). Transport rankings of non-steroidal antiinflammatory drugs across blood-brain barrier in vitro models. PLoS One *9*, e86806.

Obradovic, T., Dobson, G.G., Shingaki, T., Kungu, T., and Hidalgo, I.J. (2007). Assessment of the first and second generation antihistamines brain penetration and role of P-glycoprotein. Pharm. Res. *24*, 318–327.

Okano, H., and Yamanaka, S. (2014). iPS cell technologies: significance and applications to CNS regeneration and disease. Mol. Brain *7*, 22.

Orlova, V.V., van den Hil, F.E., Petrus-Reurer, S., Drabsch, Y., Ten Dijke, P., and Mummery, C.L. (2014). Generation, expansion and functional analysis of endothelial cells and pericytes derived from human pluripotent stem cells. Nat. Protoc. *9*, 1514–1531.

Perriere, N., Yousif, S., Cazaubon, S., Chaverot, N., Bourasset, F., Cisternino, S., Decleves, X., Hori, S., Terasaki, T., Deli, M., et al. (2007). A functional in vitro model of rat blood-brain barrier for molecular analysis of efflux transporters. Brain Res. *1150*, 1–13.

Piontek, J., Fritzsche, S., Cording, J., Richter, S., Hartwig, J., Walter, M., Yu, D., Turner, J.R., Gehring, C., Rahn, H.P., et al. (2011). Elucidating the principles of the molecular organization of heteropolymeric tight junction strands. Cell Mol. Life Sci. *68*, 3903–3918.

Protze, J., Eichner, M., Piontek, A., Dinter, S., Rossa, J., Blecharz, K.G., Vajkoczy, P., Piontek, J., and Krause, G. (2015). Directed structural modification of *Clostridium perfringens* enterotoxin to enhance binding to claudin-5. Cell Mol. Life Sci. *72*, 1417–1432.

Reinhardt, P., Glatza, M., Hemmer, K., Tsytsyura, Y., Thiel, C.S., Hoing, S., Moritz, S., Parga, J.A., Wagner, L., Bruder, J.M., et al. (2013). Derivation and expansion using only small molecules of human neural progenitors for neurodegenerative disease modeling. PLoS One *8*, e59252.

Takeuchi, T., Yoshitomi, S., Higuchi, T., Ikemoto, K., Niwa, S., Ebihara, T., Katoh, M., Yokoi, T., and Asahi, S. (2006). Establishment and characterization of the transformants stably-expressing MDR1 derived from various animal species in LLC-PK1. Pharm. Res. *23*, 1460–1472.

Vastag, M., and Keseru, G.M. (2009). Current in vitro and in silico models of blood-brain barrier penetration: a practical view. Curr. Opin. Drug Discov. Dev. *12*, 115–124.

Warren, M.S., Zerangue, N., Woodford, K., Roberts, L.M., Tate, E.H., Feng, B., Li, C., Feuerstein, T.J., Gibbs, J., Smith, B., et al. (2009). Comparative gene expression profiles of ABC transporters in brain microvessel endothelial cells and brain in five species including human. Pharmacol. Res. *59*, 404–413.

Weksler, B.B., Subileau, E.A., Perriere, N., Charneau, P., Holloway, K., Leveque, M., Tricoire-Leignel, H., Nicotra, A., Bourdoulous, S., Turowski, P., et al. (2005). Blood-brain barrier-specific properties of a human adult brain endothelial cell line. FASEB J. *19*, 1872–1874.

Wolburg, H., Neuhaus, J., Kniesel, U., Krauss, B., Schmid, E.M., Ocalan, M., Farrell, C., and Risau, W. (1994). Modulation of tight junction structure in blood-brain barrier endothelial cells Effects of tissue culture, second messengers and cocultured astrocytes. J. Cell Sci. *107*, 1347–1357.

Yan, Y., Shin, S., Jha, B.S., Liu, Q., Sheng, J., Li, F., Zhan, M., Davis, J., Bharti, K., Zeng, X., et al. (2013). Efficient and rapid derivation of primitive neural stem cells and generation of brain subtype neurons from human pluripotent stem cells. Stem Cells Transl. Med. *2*, 862–870.

Yu, J., Vodyanik, M.A., Smuga-Otto, K., Antosiewicz-Bourget, J., Frane, J.L., Tian, S., Nie, J., Jonsdottir, G.A., Ruotti, V., Stewart, R., et al. (2007). Induced pluripotent stem cell lines derived from human somatic cells. Science *318*, 1917–1920.

Yusof, S.R., Avdeef, A., and Abbott, N.J. (2014). In vitro porcine blood-brain barrier model for permeability studies: pCEL-X software pKa(FLUX) method for aqueous boundary layer correction and detailed data analysis. Eur. J. Pharm. Sci. *65*, 98–111.

Zhao, R., and Pollack, G.M. (2009). Regional differences in capillary density, perfusion rate, and P-glycoprotein activity: a quantitative analysis of regional drug exposure in the brain. Biochem. Pharmacol. *78*, 1052–1059.